Oxidation mechanism and valence states of copper and manganese in tetragonal $CuMn_2O_4$

Bernard Gillot,* Stephane Buguet and Etienne Kester

Laboratoire de Recherches sur la Réactivité des Solides, UMR 5613 CNRS, Université de Bourgogne, BP400, 21011 Dijon Cedex, France

With the view of determining the ionic configuration in tetragonal $CuMn_2O_4$ spinels prepared between 850 and 930 °C, the valence states of copper and manganese and the oxidation mechanism of these compounds have been determined by XPS, FTIR spectroscopy analyses and DTG measurements. For unoxidized samples, XPS spectroscopy analysis shows a predominately monovalent copper located in tetrahedral sites. Divalent copper in octahedral sites is also present, but at a lower level. Similar results are obtained for oxidized samples. FTIR data, upon oxidation of Cu and Mn ions below 500 °C, confirm the formation of a metastable spinel phase $Cu_{1.5}Mn_{1.5}O_4$ with a 1 : 3 ordering on the octahedral sublattice. A quantitative analysis by DTG mainly based on the difference of reactivity of Cu and Mn ions allows measurement of the content of each cation and determination of the ionic configuration.

In oxide spinels containing more than one transition-metal ion per formula unit, the distribution and valence states of the cations among both the tetrahedral (A sites) and octahedral (B sites) sublattices of the spinel structure, continue to be a serious problem. Concerning $CuMn_2O_4$ spinel, which we investigate here, the most likely cation distribution reported in the literature by several authors using diverse techniques indicates predominantly the presence of Cu^+ and Mn^{2+} ions at A sites and Cu^{2+}, Mn^{3+} and Mn^{4+} ions at B sites leading to an ionic configuration:[1,2]

$$(Cu^{+}_{\alpha}Mn^{2+}_{1-\alpha})_A(Cu^{2+}_{1-\alpha}Mn^{3+}_{\alpha}Mn^{4+})_BO^{2-}_4 \quad (1)$$

This distribution is essentially supported by the high electrical conductivity for this spinel having B sites containing both Mn^{3+} and Mn^{4+} ions,[3–6] a tetragonal deformation[1,2,7] owing to the presence of two Jahn–Teller ions (Cu^{2+} and Mn^{3+}) and the assumption that the ground state of copper ions in the A sites are the Cu^+ ions together with the occurrence of Mn^{4+} and Cu^{2+} ions in the B sites.[8] The presence of a small amount of Mn^{3+} ions in A sites has also to be taken into account[8,9] and in this case the ionic configuration is represented by the formula:

$$(Cu^{+}_{\alpha}Mn^{2+}_{\beta}Mn^{3+}_{1-\alpha-\beta})_A(Cu^{2+}_{1-\alpha}Mn^{3+}_{1-\beta}Mn^{4+}_{\alpha+\beta})_BO^{2-}_4 \quad (2)$$

In fact, because the ionic configuration follows the equilibrium:

$$Cu_A^{+} + Mn_B^{4+} \rightleftarrows Cu_B^{2+} + Mn_A^{3+} \quad (3)$$

which lies to the left hand side at low temperature, the compound $CuMn_2O_4$ must therefore be represented by the most probable formula (1) or (2). Cocke *et al.*[10] have provided first direct X-ray photoelectron spectroscopic evidence for the existence of a solid-state charge transfer of type (3) in a 'amorphous' $CuMn_2O_4$ catalyst.

Another equilibrium which influences the ionic configuration is pure electronic exchange:

$$Mn_A^{3+} + Mn_B^{3+} \rightleftarrows Mn_A^{2+} + Mn_B^{4+} \quad (4)$$

which is supposed to be shifted to the right for the manganese-rich compounds.[8] This assumption requires a $Mn_A^{3+/2+}$ redox couple of lower energy than the $Mn_B^{4+/3+}$ redox couple, which is not unreasonable in view of the surface disproportionation reaction:

$$2Mn_B^{3+} \rightleftarrows Mn_{solution}^{2+} + Mn_B^{4+} \quad (5)$$

that takes place on the spinel $LiMn_2O_4$.[11]

In a previous work[12] we have reported on the stability of solid solutions $Cu_xMn_{3-x}O_4$ ($0 \leqslant x < 1$) in air. According to the phase diagram,[2] these solid solutions are unstable below 750 °C leading to a copper-rich spinel in the presence of α-Mn_2O_3 as a result of oxygen contamination. For $CuMn_2O_4$ the oxidation reaction can be written:

$$CuMn_2O_4 + [y/(4+4y)]O_2 \rightarrow [1/(1+y)]Cu_{1+y}Mn_{2-y}O_4 + [(2+2y)/4y]Mn_2O_3 \quad (6)$$

For a complete oxidation ($y = 0.5$) and according to formula (1), the oxidation mechanism may be depicted by the following reaction:

$$(Cu^{+}_{\alpha}Mn^{2+}_{1-\alpha})_A(Cu^{2+}_{1-\alpha}Mn^{3+}_{\alpha}Mn^{4+})_BO^{2-}_4 + [(3-2\alpha)/12]O_2 \rightarrow 2/3\alpha(Cu^{+})_A(Cu^{2+}_{0.5}Mn^{4+}_{1.5})_BO^{2-}_4 + [(3-2\alpha)/2]Mn_2O_3 \quad (7)$$

This distribution suggested the contribution of two oxidation reactions compatible to:

$$\alpha Cu^{+} \rightarrow \alpha/3Cu^{2+} + 2\alpha/3Cu^{+} \quad (8)$$

with the oxidation of 1/3 of the Cu^+ ions and

$$(1-\alpha)Mn^{2+} + (2-\alpha)Mn^{3+} \rightarrow (3-2\alpha)Mn^{3+} \quad (9)$$

with the total oxidation of the Mn^{2+} ions.

Here, we report an investigation by derivative thermogravimetry (DTG) of the cation distribution in $CuMn_2O_4$ prepared by a conventional ceramic route at temperatures between 850 and 930 °C where the two cations, copper and manganese, can be oxidized sucessively.[13] This method, which is based on the difference in reactivity toward oxygen of oxidizable cations in relation to occupied sites, is especially suited to this purpose owing to the fact that it is possible to carry out a systematic study of the oxidation process with regard to the nature, charge and position of cations in the spinel lattice.[14] XPS and FTIR spectroscopic measurements were also investigated for stoichiometric and oxidative non-stoichiometric compounds in order to obtain information on the one hand about the valence states of copper and on the other about the presence of an ordered distribution.

Experimental

Polycrystalline samples with the final chemical composition $CuMn_2O_4$ were prepared by prolonged grinding using agate mortars and pestles of appropriate quantities of pure oxides CuO and Mn_2O_3 and sintering of the mixture for 48 h in air at temperatures between 930 and 850 °C. The sequence of grinding (which provides highly reactive materials) and sintering was repeated until a homogeneous single phase was obtained. This single phase material could only be obtained by quenching the specimen in water. Such treatment at high temperature has been found to cause an increase of the crystallite size since the average diameter observed from electron microscopy was of the order of 3–4 μm.

$Cu_{1.5}Mn_{1.5}O_4$ was prepared by coprecipitation of copper and manganese salts in oxalic acid as reported in ref. 15. $LiMn_2O_4$ was prepared by heating a mixture of lithium and manganese carbonates at 710 °C in air for 48 h, followed by grinding and reheating for 24 h at 740 °C.

XRD analyses were performed using a Rigaku 18 kW rotating anode diffraction system equipped with a Cu-target anode. α-Quartz was used as an external calibration standard. For the precise determination of the lattice parameters, X-ray reflections in the range θ 20–50° were recorded by step scanning, using increments of 0.01 °θ and a fixed counting time of 60 s step^{-1}. The error in the measured lattice parameter resulting from sample positioning and instrument precision is estimated to be ±0.0003 nm.

The oxidation reactions were performed in a Setaram MTB 10–8 microbalance (symmetrical set-up, resolution and noise level *ca.* 0.1 μg) with the temperature increasing at a linear rate (2 °C min^{-1}) and using powdered samples (10 mg) ground in an agate vibration mill. For a ground sample for 10 min the grain size was about 0.3 μm.

The differential scanning calorimetry experiments were carried out under air with a Setaram DSC 111G using *ca.* 60 mg of fine powder. In both the DTG and DSC experiments the base line, measured under identical conditions, was subtracted from the measured values.

The IR spectra were recorded with a Perkin-Elmer 1725X FTIR spectrometer over the range 4000–400 cm^{-1} and with a Perkin-Elmer 1700 FTIR spectrometer over the range 500–50 cm^{-1}. Ground sample (1 mg) was mixed with 200 mg of spectroscopically pure dry CsI and pressed into disks before the spectra were recorded.

X-Ray photoelectron spectroscopy (XPS) results were obtained with a Riber spectrometer AES-ESCA-ELS MAG2 instrument equipped with an Al anode operating at 13 kV and 20 mA current emission ($h\nu$ = 1486.6 eV). Binding energies were determined from a C 1s peak at 284.7 eV and manganite powder was pressed into a piece of indium foil (99.999%) that was grounded to the spectrometer in the examination. Some of the samples were irradiated with X-rays several times to check if the measurement itself gives rise to changes in the distribution of the oxidation states of the analysed elements; no changes in the spectra were observed.

Results and Discussion

Unoxidized samples

The spinels prepared in the temperature range 850–930 °C are slightly tetragonal at room temperature as shown in Fig. 1. When the preparation temperature was increased, the tetragonal axial *c*/*a* ratio decreased which can be attributed to a change in cation distribution modifying the number of distorting ions such as Mn^{3+} and Cu^{2+}.[8]

Fig. 2 shows FTIR spectra of samples for different preparation temperatures. All the spectra exhibit two broad absorption bands near 480 and 600 cm^{-1} typical of a chemical

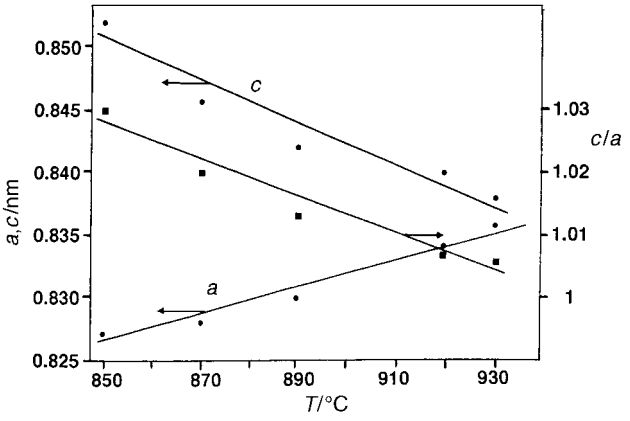

Fig. 1 Lattice parameters *a* and *c* and the *c*/*a* ratio of $CuMn_2O_4$ spinel determined as a function of the preparation temperature

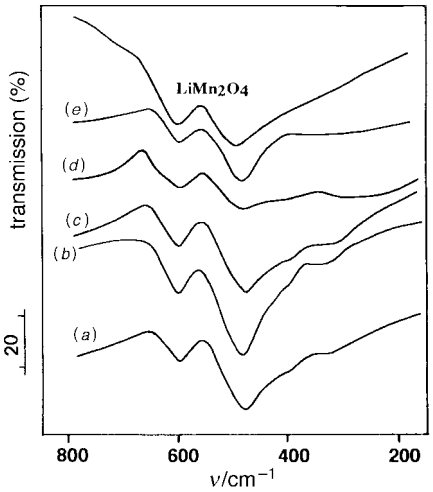

Fig. 2 FTIR spectrum of $CuMn_2O_4$ for different preparation temperatures: (*a*) 850 °C, (*b*) 870 °C, (*c*) 890 °C, (*d*) 910 °C, (*e*) 930 °C. The spectrum of $LiMn_2O_4$ is given for comparison.

disorder resulting from Mn^{3+} and Mn^{4+} ions on equivalent B sites.[16] The IR spectrum of $LiMn_2O_4$ with the cation distribution $(Li^+)_A(Mn^{3+}Mn^{4+})_BO^{2-}{}_{4\alpha}$ also consists of two featureless bands centered at 611 and 506 cm^{-1} (Fig. 2). These bands have been interpreted as being composed of contributions from tetrahedral LiO_4 units (600–650 cm^{-1}) and octahedral MnO_6 units (450–550 cm^{-1}).[17] We can thus postulate, because the difference in charge and covalency between copper and manganese cations is sufficiently great, that the absorption band at 600 cm^{-1} may be associated with CuO_4 units where the ionisation state of copper is likely to be Cu^+.

Fig. 3 shows XPS spectra of $CuMn_2O_4$ in the copper $2p_{3/2}$ region. For the spinels prepared at 850 and 870 °C [Fig. 3(*a*) and (*b*)] the Cu $2p_{3/2}$ peak contains two distinct signals. The signal at 931.3 eV is due to monovalent copper in accord with previously reported data.[18] The signal of lower intensity at 933.9 eV together with its satellite between 939–946 eV are indicative of divalent copper.[19] For the spinels prepared at 890 and 930 °C [Fig. 3(*c*) and (*d*)], curve fitting yields also two signals arising from Cu^+ and Cu^{2+} ions. Yoon and Cocke[20] and more recently Töpfer *et al.*[21] recorded the Cu 2p spectrum of CuNi manganite spinels and have attributed the signal at 931.2 eV to Cu^+ ions on tetrahedral sites and the signal at higher binding energy (934 eV) to the presence of Cu^{2+} ions on octahedral sites. We conclude that whatever the temperature of preparation the majority of the copper ions occupy tetrahedral sites and are in the monovalent state. From these measurements, if we compare the ratio of the resolved

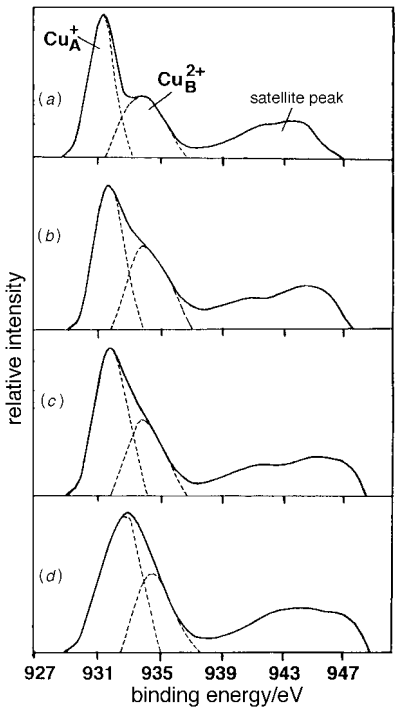

Fig. 3 Cu $2p_{3/2}$ spectrum of $CuMn_2O_4$ for different preparation temperatures: (*a*) 850 °C, (*b*) 870 °C, (*c*) 890 °C, (*d*) 930 °C

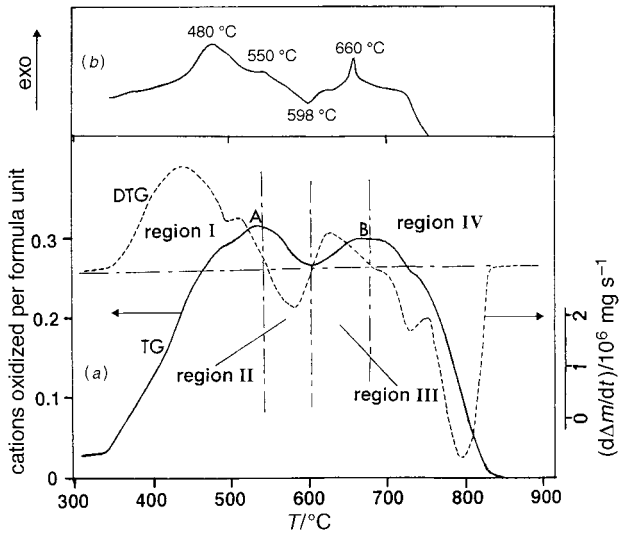

Fig. 4 Thermal behavior of $CuMn_2O_4$ prepared at 890 °C. (*a*) TG and DTG curves, (*b*) DSC curve.

Cu^{2+}/Cu^+ components (considering that the satellite area is included in the Cu^{2+} component) for the various copper manganites, it can be concluded that the copper species ratios (close to 1.50) vary little. One can argue that this ratio is only an estimate of the atomic ratio of species in the bulk since the stoichiometry or species ratio might vary with depth into the specimen; under such circumstances the XPS data would not accurately reflect the bulk configuration. The identification of three Mn species in the copper manganite (Mn^{2+}, Mn^{3+}, Mn^{4+}) has been not possible in this study owing to the existence of charging effects which probably result in line broadening for Mn 3p and Mn 2p spectra. Such effects have already been reported for many manganese compounds.[10,22]

Oxidized samples

Thermal behavior under a pure oxygen pressure of 4×10^5 Pa. Fig. 4(*a*), shows the TG curve between 300 and 900 °C and indicates four regions. In the initial temperature range (region I) a mass gain is observed on heating. This gain starts above 300 °C and reaches a maximum near 540 °C. In region II, between 540 and 600 °C, a continuous mass loss is detected. Above 600 °C, the TG curve was again characterized by an oxidation domain (region III) and finally by a mass loss beyond 700 °C (region IV) that restores the initial stoichiometry of the sample. The DSC curve [Fig. 4(*b*)] exhibits three oxidation peaks at 480, 550 and 660 °C and a reduction peak at 600 °C. The high-temperature (HT) spinel phase does not pick up oxygen on the timescale of cooling (10 °C min^{-1}). We therefore distinguish this HT spinel from the initial spinel phase. Although the thermal behavior of $CuMn_2O_4$ has been studied by several researchers,[6,23–25] the distribution and valence of the transition-metal ions by derivative thermogravimetry and thereby the oxidation mechanism has not been determined.

Fig. 4(*a*) also shows the corresponding DTG curve, where for regions I and IV, two separate stages can be distinguished. The same behavior was also observed at various treatment temperatures (Fig. 5). Identification of two separate stages, which can be clearly seen after deconvolution, has important consequences with regard to the oxidation states of the cations because it is possible to attribute for each oxidizable cation, not only a characteristic oxidation temperature but also to determine from the area of each peak, the populations of oxidized or reduced ions.[26]

Based on these considerations, the first peak observed in region I at *ca.* 425 °C represents the oxidation of Cu^+ ions at A sites and the second centered at *ca.* 500 °C can be explained in terms of the oxidation of manganese ions located at the same sites. Such an assignment would account for the established inverse relation between oxidation temperature and the invariance on the cation–oxygen distance in tetrahedral or octahedral sites as previously shown for several copper- or manganese-based spinel oxides.[13] For the A sites, these cation–oxygen distances are Cu^+—O 0.2086, Mn^{2+}—O 0.2041 and

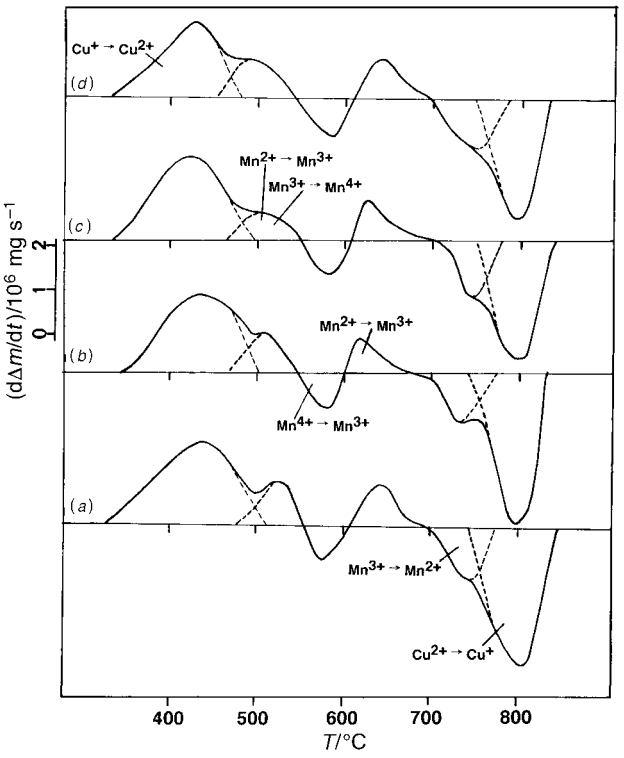

Fig. 5 DTG curves recorded on $CuMn_2O_4$ for different preparation temperatures: (*a*) 850 °C, (*b*) 870 °C, (*c*) 890 °C, (*d*) 930 °C. The deconvolution of the oxidation (region I) and reduction (region IV) peaks is shown.

Mn^{3+}—O 0.1891 nm. However, the oxidation of the manganese ions requires a careful consideration from the fact this cation yields a redox process on heating in air above 500 °C.[27] It has been demonstrated that for the Mn-based spinels, the Mn^{4+} ions formed during the oxidation of Mn^{2+} and Mn^{3+} ions at low temperature are unstable beyond 500–550 °C and that an inevitable reduction takes place in the temperature range 550–600 °C. It is logical, therefore, to assign the peak of region II at the reduction of Mn^{4+} to Mn^{3+} ions as established for the decomposition of MnO_2 into Mn_2O_3.[28] In region III, the mass gain corresponds to the oxidation of Mn^{2+} ions not being completely oxidized in region I, as already found in many manganese iron spinels.[13] Above 700 °C mass loss occurs following two distinct processes as clearly shown by the DTG curves.

Identification of formed phases. In order to identify the formed phases, FTIR spectra were measured on heating the spinel separately in a furnace at different selected temperatures for 10 min and then quenching. In contrast to the spectrum of a sample heated below 500 °C [Fig. 6(*a*)–(*c*)], the spectra of samples oxidized at 500 and 550 °C [Fig. 6(*d*), (*e*)] show the presence of a large number of absorption bands suggesting an octahedral ordering[8,15] to give the spinel of ionic configuration $(Cu^{+})_A(Cu^{2+}{}_{0.5}Mn^{4+}{}_{0.5})_BO^{2-}{}_4$. A close similarity was observed with the spectrum of an ordered $Cu_{1.5}Mn_{1.5}O_4$ spinel heated at 500 °C (Fig. 6) where in a number of studies this spinel is quoted to have an ionic 1:3 ordering in the B sublattice. Unfortunately the superstructure line in the X-ray diffraction pattern could not be found owing to the similar X-ray scattering power of Cu and Mn.

Concerning the presence of Mn_2O_3 that accompanied the ordered spinel in region I according to reaction (6), it should be considered that oxidation will rather take place through the segregation of γ-Mn_2O_3 instead of α-Mn_2O_3 which only results in broadening of the X-ray diffraction lines as observed experimentally. The former modification of Mn_2O_3 has a spinel structure where vacancies are mainly located on A sites and can be attributed to the clustering of the distorting Jahn–Teller ions such as Mn^{3+}, which plays an important role in the stability and the homogeneity of the spinel structure.[29]

At higher temperature, 630 °C, no fine structure is observed in the spectrum [Fig. 6(*f*)] indicating that the spinel is disordered as already reported by Jarrigue and Mexmain[15] and exemplified here for a $Cu_{1.5}Mn_{1.5}O_4$ spinel quenched from 650 °C (Fig. 6). A new absorption band centered at *ca.* 590 cm^{-1} is present which is likely associated with the formation of α-Mn_2O_3 resulting from the γ-$Mn_2O_3 \rightarrow \alpha$-$Mn_2O_3$ transformation. Above 700 °C, when the $Cu_{1.5}Mn_{1.5}O_4$ and α-Mn_2O_3 react to give the stoichiometric spinel $CuMn_2O_4$ [Fig. 6(*g*), (*h*)], two absorption bands at *ca.* 600 and 480 cm^{-1} are seen.

In the course of this study it was deemed necessary to determine the oxidation states of copper under different thermal treatments by XPS. In Fig. 7 it can be seen that the 2p spectrum of copper at room temperature for an initial $Cu_{1.5}Mn_{1.5}O_4$ spinel [curve (*a*)] a $CuMn_2O_4$ heated at 540 °C [curve (*b*)] and a $CuMn_2O_4$ heated at 670 °C [curve (*c*)] can be resolved into components representing the contributions of Cu^{+} and Cu^{2+} species. In comparison with an initial $Cu_{1.5}Mn_{1.5}O_4$ spinel, we conclude that for the two selected temperatures corresponding to maxima A and B in the TG curve (Fig. 4), Cu^{+} in A sites and Cu^{2+} in B sites predominate in oxidized samples and that for regions I, II and III monovalent copper must be present as well. This proves that Cu^{+} ions are only partially oxidized below 700 °C excluding the occurrence of tetrahedral divalent copper.

Ionic configuration. At point A, it can be observed from Fig. 8(*b*)–(*e*) that longer grinding times lead to a greater reaction rate and degree of oxidation. With increased grinding time, the average oxidation state of the manganese and copper

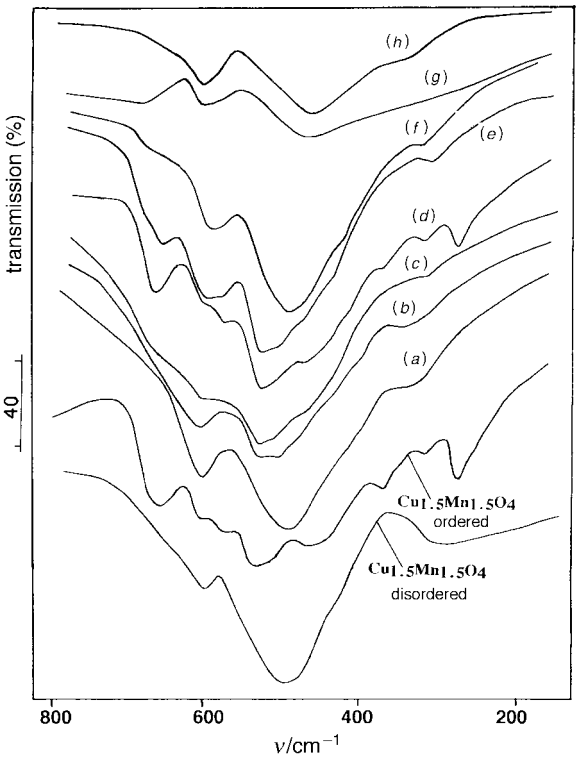

Fig. 6 FTIR spectra of $CuMn_2O_4$ prepared at 890 °C oxidized under $P(O_2)=4\times10^5$ Pa at different temperatures. Each curve corresponds to oxidation with the temperature increasing at a linear rate of 2 °C min^{-1} and then quenched. (*a*) 200 °C, (*b*) 300 °C, (*c*) 400 °C, (*d*) 500 °C, (*e*) 550 °C, (*f*) 630 °C, (*g*) 800 °C, (*h*) 900 °C. The FTIR spectrum of ordered and disordered $Cu_{1.5}Mn_{1.5}O_4$ is given for comparison.

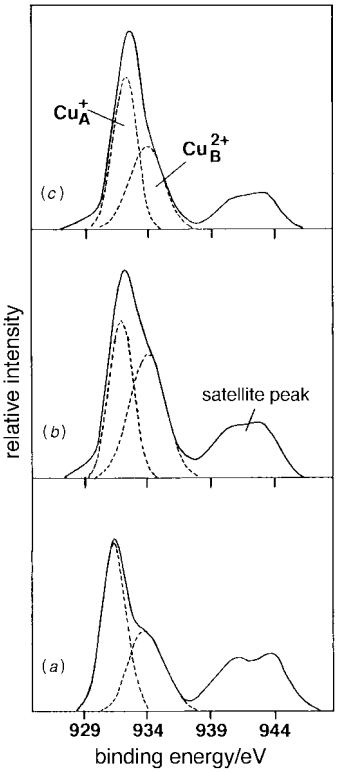

Fig. 7 Cu $2p_{3/2}$ spectrum of: (*a*) initial $Cu_{1.5}Mn_{1.5}O_4$, (*b*) $CuMn_2O_4$ oxidized at 540 °C, (*c*) $CuMn_2O_4$ oxidized at 670 °C

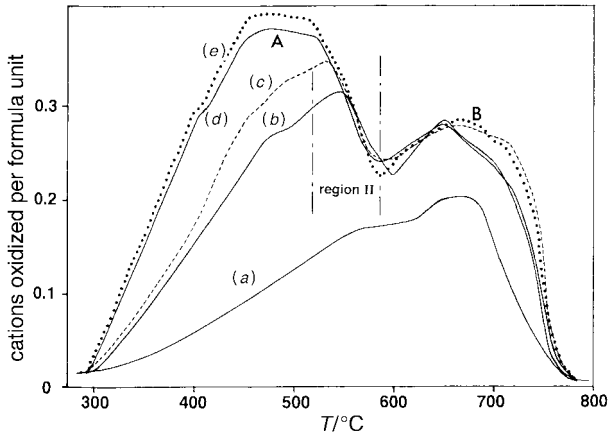

Fig. 8 TG curves showing the effect of grinding time on the oxidation behavior of $CuMn_2O_4$ prepared at 890 °C: (*a*) unground sample, (*b*) 10 min, (*c*) 12 min, (*d*) 15 min, (*e*) 18 min grinding time

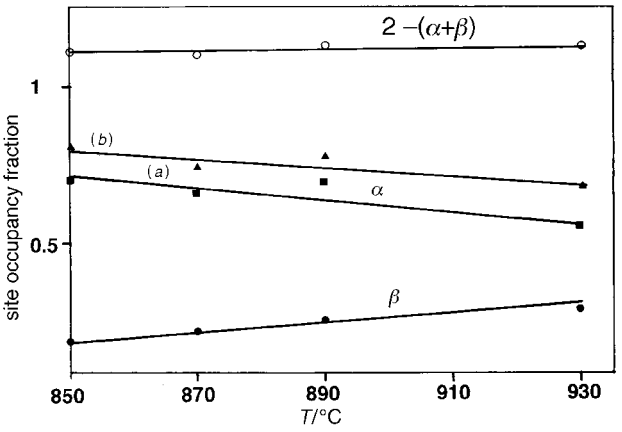

Fig. 9 Site occupancy fraction of Cu_A (α), $Mn_A{}^{2+}$ (β) and $Mn^{3+}+Cu^{2+}$ on B sites $[2-(\alpha+\beta)]$ as a function of the preparation temperature: (*a*) site occupancy fraction of Cu^+ ion deduced from reduction peak, (*b*) site occupancy fraction of Cu^+ ion deduced from oxidation peak.

increase resulting essentially in formation of a greater number of Mn^{4+} ions and consequently explains the greater observed amount of reduced Mn^{4+} ions in region II. Such a decrease was not seen in an unground sample [Fig. 8(*a*)] precluding the absence of Mn^{4+} ions produced by oxidation in region I. It should be noted that the oxygen excess δ for $Cu_{1.5}Mn_{1.5}O_{4+\delta}$, which would indicate the presence of cation vacancies, remains low and that the metastability of the spinel phase below 500 °C would be predominantly associated with oxidation of Mn^{2+} and Mn^{3+} to Mn^{4+}. The existence of high oxidation states in Mn-containing spinels implies, for finely divided samples, the presence of cation vacancies in the spinel structure. It is commonly found that the oxidation of Mn_3O_4 spinel may lead to the formation of a non-stoichiometric spinel with a higher cation vacancy content that in γ-Mn_2O_3.[29]

In contrast to point A, a close similarity in the oxidized amounts was observed for ground samples for the second maximum indicating that the formed phases at higher temperature in the interval $670<T/°C<700$ is not due to kinetic factors, but is thermodynamically controlled where the stable phases are $Cu_{1.5}Mn_{1.5}O_4$ and α-Mn_2O_3. Therefore, in an ideal simplified case, the reduction of these oxides is the most appropriate means to determine the ionic configuration in assuming that the formed spinel at the plateau region ($T>800$ °C) is stoichiometric. It should be noted, however, that the mass loss is associated in the first step with the reduction of Mn^{3+} ions and in the second step with the reduction of Cu^{2+} ions. The reaction that occurs between 700 and 800 °C in the DTG curves is therefore proposed to be the inverse of reactions (8) and (9). The two separate reduction stages fitted in region IV allow calculation of the content of each reduced cation from the area of each peak. This was done following the procedure indicated in ref. 14 by calculating the S_i/S_o ratio, where S_i represents the area of each peak and S_o the area corresponding to the standard oxidation peak of Fe_3O_4 spinel which allows a direct comparison between the samples. Fig. 9 shows the experimentally determined values α [curve (*a*)] and β of the site occupancy fraction per molecule for each reduced cation. From these values an ionic configuration based on formula (2) which takes into account the presence of a small amount of Mn^{3+} ions on A sites can be determined as a function of the preparation temperature. It is interesting that the concentration of Cu^+ ions can also be calculated from the first oxidation peak. As can be clearly seen from the α values shown in Fig. 9(*b*), the site occupancy fraction was larger than that obtained for the reduction peak. This effect can be attributed to the formation of a $Cu_{1.5}Mn_{1.5}O_{4+\delta}$ spinel phase where the excess oxidation δ is accommodated as cation vacancies.

The magnitude of the c/a ratio, which reflects the extent of the Jahn–Teller distortion, depends on the concentration of Mn^{3+} and Cu^{2+} ions on the octahedral sites. As can be observed from Fig. 9, there is a slight change of the $[2-(\alpha+\beta)]$ value (*i.e.*, the $Cu^{2+}+Mn^{3+}$ ions content on B sites) associated with the decrease in the c/a ratio (Fig. 1).

References

1 R. Buhl, *J. Phys. Chem. Solids*, 1969, **30**, 28.
2 R. E. Vandenbergue, G. G. Robbrecht and V. A. M. Brabers, *Mater. Res. Bull.*, 1973, **8**, 571.
3 C. D. Sabane, V. B. Tare and A. P. B. Sinha, *Indian J. Pure Appl. Phys.*, 1967, **5**, 213.
4 S. T. Kshirsagar, *J. Phys. Soc. Jpn*, 1969, **27**, 1164.
5 B. Gillot, M. Kharroubi, R. Metz, R. Legros and A. Rousset, *Phys. Status Solidi A*, 1991, **124**, 317.
6 J. Töpfer and A. Feltz, *J. Alloys Compd.*, 1993, **202**, 231.
7 R. Metz, J. P. Caffin, R. Legros and A. Rousset, *J. Mater. Sci.*, 1989, **24**, 83.
8 A. D. D. Broeme and V. A. M. Brabers, *Solid State Ionics*, 1985, **16**, 171.
9 R. E. Vandenbergue, G. G. Robbrecht and V. A. M. Brabers, *Phys. Status Solidi A*, 1976, **34**, 583.
10 D. L. Cocke and S. Veprek, *Solid State Commun.*, 1986, **57**, 745.
11 J. C. Hunter, *J. Solid State Chem.*, 1981, **39**, 142.
12 B. Gillot, M. Kharroubi, R. Metz, R. Legros and A. Rousset, *J. Solid State Chem.*, 1991, **91**, 375.
13 B. Gillot, V. Nivoix, E. Kester, O. Nusillard, C. Villette, Ph. Tailhades and A. Rousset, *Mater. Chem. Phys.*, 1997, **48**, 111.
14 B. Gillot, *J. Solid State Chem.*,1994, **113**, 163.
15 J. Jarrigue and J. Mexmain, *Bull. Soc. Chim. Fr.*, 1980, **9–10**, 363.
16 B. Gillot, *Vibr. Spectrosc.*, 1994, **6**, 127.
17 T. J. Richardson and P. N. Ross, Jr., *Mater. Res. Bull.*, 1996, **31**, 935.
18 M. Lenglet, A. D'Huysser, J. Kasperek, J. P. Boulle and J. Dürr, *Mater. Res. Bull.*, 1985, **20**, 745.
19 R. Hahn and S. Storp, *Appl. Phys.*, 1976, **9**, 217.
20 C. Yoon and D. L. Cocke, *J. Catal.*, 1988, **113**, 267.
21 J. Töpfer, A. Feltz, D. Gräf, B. Hackl, L. Raupach and P. Weissbrodt, *Phys. Status Solidi A*, 1992, **134**, 405.
22 T. Hashemi, *Br. Ceram. Trans. J.*, 1991, **90**, 171.
23 J. Jarrige and J. Mexmain, *Bull. Soc. Chim. Fr.*, 1976, 405.
24 L. S. Puckhaber, H. Cheung, D. L. Cocke and A. Clearfield, *Solid State Ionics*, 1989, **32/33**, 206.
25 R. Metz, J. P. Caffin, R. Legros and A. Rousset, *J. Mater. Sci.*, 1989, **24**, 83.
26 E. Kester, B. Gillot, P. Perriat, Ph. Dufour, C. Villette, Ph. Tailhades and A. Rousset, *J. Solid State Chem.*, 1996, **126**, 7.
27 B. Gillot, M. El Guendouzi, Ph. Tailhades and A. Rousset, *React. Solids*, 1986, **1**, 139.
28 E. M. Vogel, D. W. Johnson and P. K. Gallagher, *J. Am. Ceram. Soc.*, 1977, **60**, 31.
29 J. Kacmarek and E. Wolska, *J. Solid State Chem.*, 1993, **103**, 387.

Paper 7/037131G; *Received* 29*th May*, 1997